



Article

Mass Balance of the Antarctic Ice Sheet in the Early 21st Century

Tian Yang, Qi Liang * , Lei Zheng, Teng Li , Zhuoqi Chen, Fengming Hui and Xiao Cheng

School of Geospatial Engineering and Science, Sun Yat-sen University, Southern Marine Science and Engineering Guangdong Laboratory (Zhuhai), Zhuhai 519082, China

* Correspondence: liangq57@mail.sysu.edu.cn

Abstract: Mass loss from the Antarctic Ice Sheet (AIS) is an important contributor to global sea level rise. To examine the recent ice loss, we estimated the mass budget of the AIS from 2000 to 2020 using multiple ice velocity datasets, state-of-the-art ice thickness datasets, and extended surface mass balance (SMB) records. The AIS lost mass at an average rate of -89 ± 99 Gt/yr over the study period. The East Antarctic Ice Sheet (EAIS) showed a slightly positive mass balance, while the West Antarctic Ice Sheet (WAIS) experienced a significant acceleration in mass loss. The ice discharge from the AIS increased from 1792 ± 47 Gt/yr in 2000 to 1940 ± 37 Gt/yr in 2017–2020, with the increase in the discharge from the WAIS being three to four times higher than that from the EAIS. Moreover, the average mass balance for 2017–2020 was -99 ± 93 Gt/yr, slightly more negative than the average for the early 21st Century. During this recent period, the ice discharge decreased in the East Indian Ocean sector, in contrast to its rapid increase from 2000 to 2013–2017. However, the discharge in the Amundsen Sea sector still greatly increased from 2013–2017 to 2017–2020. Overall, our results are in agreement with recent mass balance estimates for the AIS based on gravimetry and altimetry. Our assessments of the recent AIS mass balance with the mass budget method (input-output method) will contribute to the understanding of ice dynamic processes and provide insights into the stability of the AIS.

Keywords: mass balance; ice discharge; Antarctic Ice Sheet; input-output method



Citation: Yang, T.; Liang, Q.; Zheng, L.; Li, T.; Chen, Z.; Hui, F.; Cheng, X. Mass Balance of the Antarctic Ice Sheet in the Early 21st Century. *Remote Sens.* **2023**, *15*, 1677. <https://doi.org/10.3390/rs15061677>

Academic Editor: Gareth Rees

Received: 9 February 2023

Revised: 15 March 2023

Accepted: 18 March 2023

Published: 20 March 2023



Copyright: © 2023 by the authors. Licensee MDPI, Basel, Switzerland. This article is an open access article distributed under the terms and conditions of the Creative Commons Attribution (CC BY) license (<https://creativecommons.org/licenses/by/4.0/>).

1. Introduction

Approximately 70% of the world's freshwater is stored as ice in the Antarctic Ice Sheet (AIS), and it holds enormous potential to raise global sea level by 58 m [1–3]. The AIS contributed 7.6 ± 3.9 mm to global mean sea level rise from 1992 to 2017 [4]. These freshwater ice changes can not only lead to sea level rise, but can also dramatically impact the ocean surface temperature, salinity, thermohaline circulation, and global carbon cycle [5–7]. Continuous monitoring of the mass balance of the AIS is essential for predicting sea level change. A more accurate understanding of the spatial and temporal distribution of the mass balance of the AIS, as well as how it responds to the patterns of climate change, is also essential for understanding the stability of the ice sheet.

Recent studies have shown that the AIS is losing mass mainly due to changes in ice dynamics caused by the intrusion of warmer, saltier sea water around Antarctica [8–10]. At present, various remote sensing-based methods have been used to estimate the mass balance of the AIS, including: (1) the mass budget method (or input-output method, IOM), which estimates the mass change by comparing the surface mass balance (input) of the AIS with the ice discharge (output) at the grounding line [11]; (2) the altimetry method, where the change in surface elevation of the entire AIS is measured by satellite altimeters, and the change in ice volume is translated into the mass change of the ice sheet [12]; and (3) the gravity-based method, which can obtain the time-varying signal of the Earth's gravity field directly from gravity satellites, and then invert it into the relative change in ice sheet mass [13]. Each of these methods utilizes different data sources and inherent uncertainties, resulting in large differences in the results [4]. The IOM is more

a parameterized and computationally complex method compared to the altimetry and gravity methods. However, it tends to utilize higher-resolution data (100 m to 1 km) [8]. Furthermore, the IOM is better suited for revealing the physical mass loss process, which is crucial for understanding the variations in ice mass changes across different basins of the AIS.

The IOM has long been used to assess the mass balance of the AIS [11,14,15]. Recently, Rignot et al. [8] estimated the mass balance for the entirety of Antarctica over nearly four decades from 1979–2017. An improvement to reduce the uncertainty in the discharge estimation was proposed by Gardner et al. [16]. They calculated the mass balance of the AIS for 2008–2015 using Antarctic-wide ice velocity products derived from Landsat images and analyzed the trends in velocity and discharge. Ice velocity products with a higher spatial resolution were used to estimate the mass balance of the AIS in 2008, 2014, and 2015 [17]. Other studies have used the IOM to estimate regional mass balance values at the drainage basin scale. Estimates of the mass balance of the Totten Glacier during 1989–2015 revealed a link between ice dynamic changes and ocean temperature, with a significant increase in ice velocity occurring in response to increasing ocean temperatures [18]. Assessments of the Amery Ice Shelf region show a long-term slight positive mass balance for this ice shelf basin [19–21]. A study of the Getz region in West Antarctica revealed that, from 1994 to 2008, two-thirds of the mass loss in this region was due to dynamic imbalance, which was likely related to ocean forcing [22]. From the results of the different ways to assess the mass balance published by the Ice sheet Mass Balance Inter-Comparison Exercise (IMBIE) in 2018, there are still relatively large differences among the three estimation methods. For example, for the mass balance results of the AIS from 2003–2010, the altimetry method yields -43 ± 21 Gt/yr, the gravimetry method yields -76 ± 20 Gt/yr, and the IOM yields -201 ± 82 Gt/yr [4]. Combining the results of the three methods while exploring the intrinsic relationships between them can help us better understand the causes of fluctuations in the mass balance of the AIS. The mass balance of the AIS has been estimated up to 2019 using the altimetry method [7] and up to 2020 using the gravimetry method [23]. However, the comprehensive evaluation of recent Antarctic-wide mass balance is currently lacking due to limitations in data and methodology. Estimates of the mass balance of the AIS using the IOM stopped in 2017 [8], preventing us from comparing the differences in the assessments of recent mass balance with the three methods.

In this study, we use the IOM to estimate the mass balance of the AIS up to the year 2020. We assess the mass balance variability of the AIS for individual basins from 2000 to 2020 using multiple surface velocity data products combined with surface mass balance (SMB) estimates. Additionally, in order to provide a comprehensive understanding of the mass balance of the AIS, we compare our results obtained via the IOM with the Gravity Recovery and Climate Experiment (GRACE) mass change results and altimetry-based estimates. We also investigate potential explanations for any discrepancies observed between the results obtained through different data and methods.

2. Data and Methods

2.1. Ice Velocity

The MEaSURES Annual Antarctic Ice Velocity Maps [24] provide annual maps of Antarctic ice surface velocity, assembled using optical and synthetic aperture radar (SAR) satellite data. Our study used these annual ice surface velocity data from 2000–2020. The spatial resolution of these velocity data is 1 km, and the uncertainty is ~ 1 –17 m/yr [24]. The Inter-Mission Time Series of Land Ice Velocity and Elevation (ITS_LIVE) ice velocity data derived from Landsat 4, 5, 7, and 8 imagery using the autonomous Repeat Image Feature Tracking (auto-RIFT) method were also used [16,25]. The spatial resolution of this dataset is 240 m, and the uncertainty is approximately 10 m/yr [16]. Other gaps in the coverage of the annual velocity product, especially for the regions south of 82.7°S, were filled using the MEaSURES InSAR-Based Ice Velocity Maps of Central Antarctica [26] and MEaSURES Phase-Based Antarctica Ice Velocity Map [27].

The MEaSURES data products have a broad temporal coverage and use multiple satellite platforms, and these products form the majority of the ice velocity data used in this study. Although the MEaSURES products have been able to represent the regional variation of the ice velocity well [28], there are still some missing values near the flux gate that need to be filled for the ice discharge calculation.

The Central Antarctica product was used to fill in missing velocity values located within the gap in the coverages of the satellite platforms at the pole. We assumed that the trend in velocity in these regions has been stable for a long time. The long-term velocity change rate was estimated from calculating the difference in Central Antarctica velocity between 2009 and 1997. Then, based on Central Antarctica velocity in 2009 and the long-term change rate, the missing values in each annual velocity map were calculated by a linear scaling method.

The ITS_LIVE annual products were further used to fill in missing values near the flux gate in the MEaSURES annual velocity products with the nearest neighbor method prior to 2013. Note that after this step the annual ice velocity was already relatively complete. In addition, we used MEaSURES Phase-Based Antarctica Ice Velocity Map to perform the final filling step to obtain a complete annual ice velocity mosaic. We divided the whole period into four epochs and listed ice velocity products used to calculate discharge in each of the epochs in Table 1. The ice velocity of each epoch was then estimated by averaging the annual ice velocity mosaics.

Table 1. List of the main ice velocity products and filling ice velocity products used in each of the epochs.

Epoch	MEaSURES Annual Velocity Products [24]	Fill Missing Values Products		
		Central [26]	ITS_LIVE [16]	Phase [27]
2000	2000–2001	✓	2000	✓
2007–2011	2007–2008, 2008–2009, 2010–2011	✓	2007, 2008, 2010	✓
2013–2017	2013–2014, 2014–2015 2015–2016, 2016–2017	✓	/	/
2017–2020	2017–2018, 2018–2019, 2019–2020	✓	/	/

2.2. Ice Thickness, Flux Gate, Grounding Line, and Basin Boundary

Ice thickness has been considered the most significant source of error in estimating mass balance by the IOM [3]. The most accurate ice thickness data for the AIS come from airborne radio echo sounding (RES) [1]. However, RES data are very sparse over some of the AIS, and many regions are still not well-covered; in particular, more than 80% of the grounding line (GL) zones have not been sounded [16]. To improve the accuracy of the discharge estimation, we adapted the flux gate (FG) method proposed by Gardner et al. [16] (Figure 1). The FG was positioned close to the RES flight lines to include more RES data by sacrificing proximity to the GL. We derived the ice thickness along the FG from the BedMachine v2 dataset [3] (Figure 2a). This dataset includes most airborne RES data and introduces flow velocity and SMB data to refine the thickness estimates by correcting temporal changes in surface mass balance and ice thickness using the mass conservation method. Therefore, we expect it to have a low uncertainty in the fast-flowing regions and provide the most reliable estimates for our calculation.

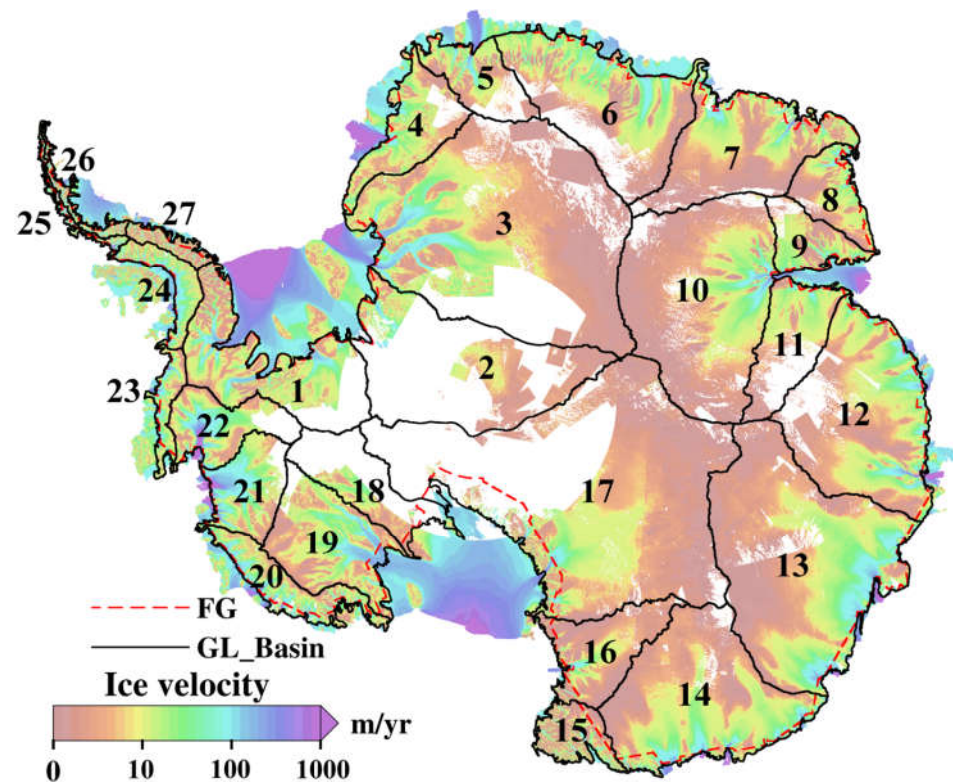


Figure 1. Ice velocity, flux gate (FG), and basin boundaries (B1–B27). The ice velocity is from the MEaSUREs annual ice velocity for 2019–2020 [24]. The red dashed line represents the FG [16], and the solid black line represents the basin boundaries and the grounding line (GL). The numbers 1–27 represent different basins [29].

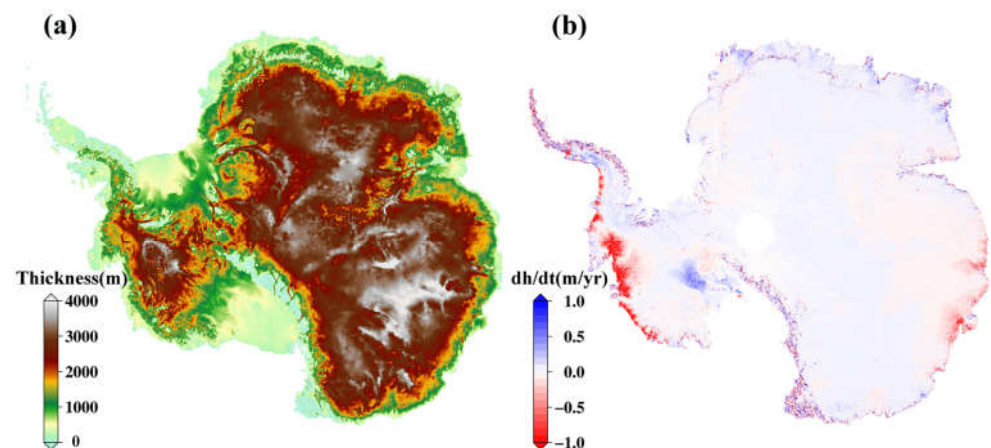


Figure 2. (a) The BedMachine ice thickness of the AIS [3]. (b) Surface elevation changes of the AIS during 2013–2020.

We defined the area of each basin by combining an updated version of the GL data [16,30] with the Antarctic basin boundary from Zwally et al. [29] (Figure 1). The continent was divided into twenty-seven basins (B1–B27), including sixteen basins in the East Antarctica Ice Sheet (EAIS: B2–B17), seven basins in the West Antarctica Ice Sheet (WAIS: B1, B18–B23), and four basins on the Antarctic Peninsula (AP: B24–B27).

2.3. Ice Discharge

For the estimation of ice discharge, the conventional approach uses the position of GL as the FG, which means the ice flux (IF) is equal to the discharge, to directly calculate the

discharge [2,8]. Because of the choice of FG, the IF and discharge are different in this study. We first discretize the FG line and then sort the FG nodes in clockwise ascending order to help determine the inflow or outflow of each FG unit (two consecutive FG nodes form an FG unit). Then, we use the ice velocity and thickness data at the location of the FG unit to estimate the IF. The calculation of the IF is expressed as follows:

$$IF = \sum_{i=1}^n H_i \cdot (V_{xi} \cdot W_{xi} + V_{yi} \cdot W_{yi}) \cdot \rho_{ice} \quad (1)$$

where n is the total number of FG units and H_i is the ice equivalent thickness. V_{xi} and V_{yi} denote the velocity components of the FG units in the x and y directions, respectively. W_{xi} is the FG projected in y coordinates and is perpendicular to V_{xi} . W_{yi} is the FG projected in x coordinates and is perpendicular to V_{yi} . ρ_{ice} is the density of ice. Here, we use 917 kg/m^3 with an uncertainty of 5 kg/m^3 in the estimation [31].

We used the following equation based on the principle of mass conservation [32] to further estimate the discharge (D) from the IF:

$$D = IF + SMB_{GL-FG} - dV_{dyn}/dt \quad (2)$$

where SMB_{GL-FG} is the unmeasured flux due to the (typically) positive surface mass balance in the region between the FG and the GL. dV_{dyn}/dt is the dynamic volume change, which is the unmeasured flux due to ice dynamics between the FG and the GL. We assume that the ice elevation only changes due to dynamic changes, and dV_{dyn}/dt can be regarded as a constant throughout the study period. We used the surface elevation change data provided by the CPOM (Centre for Polar Observation and Modelling) data portal, measured with ENVISAT and CryoSat-2 data, to calculate the dynamic volume change in each basin from 2002–2012 and 2013–2020 (Figure 2b). The CPOM elevation change data with 5 km spatial resolution are available at http://www.cpom.ucl.ac.uk/csopr/icesheets2/?icesheet_zone=antarctica accessed on 26 May 2021). The ice discharge of each epoch was estimated by averaging annual ice discharge results.

2.4. Surface Mass Balance

There are currently two conventional ways to assess the SMB of the AIS at the continental scale: either using a regional climate model (RCM) or using estimates from an atmospheric reanalysis product [33,34]. The Regional Atmospheric Climate Model (RACMO) is usually used to calculate the SMB in Antarctica [8,16,17]. Unfortunately, the latest RACMO Version 2.3p2 (RACMO2.3p2) is only available until 2017 [35]. Atmospheric reanalysis products usually include only two main SMB components: precipitation and evaporation (sublimation), with no components representing the liquid water balance [36]. Therefore, in this study, we use RACMO to assess the SMB of the AIS, and a combination of reanalysis data and RACMO to extend the SMB data to include recent years.

The spatial resolution of the outputs of the regional climate models RACMO2.3p1 and RACMO2.3p2 [35,37] is 27 km. RACMO2.3p2 is an updated version of RACMO2.3p1 that features changes to the topography, cloud scheme parameters, and snow properties [35]. We used RACMO2.3p1 to estimate the SMB values in the EAIS, as several studies have shown that RACMO2.3p1 performs better than RACMO2.3p2 in SMB estimates for the EAIS [8,38,39]. For the WAIS and the AP, we calculated the SMB using RACMO2.3p2. The SMB data product was first resampled to a grid size of 1 km. Then, the polygon vectors of individual basins (or the whole ice sheet) were masked to the grid.

The ERA5-Land product is a state-of-the-art reanalysis product, covering the period from 1950 to the present day [40]. The improvements in this recently released product include refined atmospheric physics and a revised snow scheme. We used ERA5-Land reanalysis data from 1979–2021 to extend the RACMO SMB data to 2020. We calculated the SMB from ERA5-Land by subtracting evaporation from precipitation.

For basins in the EAIS (B2–B17) in Figure 1, we used RACMO2.3p1, which only runs to 2015, and ERA5-Land data from 1979–2015 to estimate a scale factor. We calculated the total SMB from 1979–2015 for each individual basin, and the scale factor was estimated as the ratio of the SMB derived from those two datasets. Then, we scaled the SMB calculated from ERA5-Land reanalysis data to obtain the corrected SMB for the period 2015–2020. For the basins in the WAIS (B1, B18–B23) and AP (B24–B27), we performed the same calculation to extend the SMB record, but used the RACMO2.3p2 and ERA5-Land datasets from 1979–2017 to estimate the scale factor for each basin.

2.5. Mass Balance

The equation for calculating mass balance (MB) using the IOM is

$$MB = SMB - D \quad (3)$$

We use the FG defined in Section 2.3 to reduce the uncertainty in calculating the discharge (D) of the AIS. In addition, we extend the SMB of the AIS with ERA5-Land reanalysis data. The MB of the AIS for 2000–2020 is then calculated.

The discharge and SMB in the northern AP have higher uncertainty than in other regions [8]. The region has a complex basal topography and steep slopes, and the ice velocity products also have poor quality. Due to the extreme surface topography, the annual variability in precipitation and melt is also large, and the measurement of the SMB is especially challenging [16]. Therefore, we use the net mass budget results estimated from the altimetry method during the 2003–2019 period [7] to replace our mass balance estimation for B25 and B26.

2.6. Uncertainty Assessment

Uncertainty assessment of the 27 basins of the AIS needs to consider both discharge and SMB components. The different parameters are assumed to be independent in the calculation. The uncertainty in the ice flux for each basin is as follows:

$$\sigma IF = \sqrt{\sigma H^2 + \sigma V^2 + \sigma \rho_{ice}^2} \quad (4)$$

where the σIF is the uncertainty in ice flux. σH , σV , $\sigma \rho_{ice}$ are the uncertainty in ice flux that results from the uncertainty in ice thickness (H), ice velocity (V), and ice density (ρ_{ice}), respectively.

The uncertainties in ice thickness, ice velocity, and ice density are calculated as follows:

$$\sigma H = \sqrt{\sum_{i=1}^m (uH_i W_i V_i \rho_{ice})^2} \quad (5)$$

$$\sigma V = \sqrt{\sum_{i=1}^m (uV_i H_i W_i \rho_{ice})^2} \quad (6)$$

$$\sigma \rho_{ice} = \sqrt{\sum_{i=1}^m (u\rho_{ice} V_i H_i W_i)^2} \quad (7)$$

where m is the number of flux units of each basin. H_i and uH_i represent the ice thickness and uncertainty in the ice thickness for each flux unit, respectively. V_i and uV_i represent the ice surface velocity and its uncertainty, respectively. ρ_{ice} and $u\rho_{ice}$ represent the ice density and its uncertainty, respectively. W_i is the length of each flux unit perpendicular to the velocity direction.

The uncertainty in discharge in each basin can be expressed as follows:

$$\sigma D = \sqrt{\sigma IF^2 + \sigma \Delta SMB^2 + \sigma dV_{dyn}/dt^2} \quad (8)$$

Then, the uncertainty in Antarctic ice discharge is

$$\sigma D_{AIS} = \sqrt{\sum_{i=1}^n \sigma D_i^2} \quad (9)$$

where n is the number of basins. $\sigma \Delta SMB$ is the uncertainty in the SMB of the region between the GL and the FG, and $\sigma dV_{dyn}/dt$ is the uncertainty in the dynamic volume change. In this study, 20% was used to assess the uncertainty in the SMB in each basin [16]. Uncertainty in the dynamic volume change cannot be rigorously quantified. Therefore, we conservatively assumed an uncertainty of 40% of the estimated dynamic volume change magnitude.

The uncertainty in the resulting AIS mass balance estimate, σMB , is calculated as follows:

$$\sigma MB = \sqrt{\sigma D_{AIS}^2 + \sum_{i=1}^n \sigma SMB_i^2} \quad (10)$$

where σSMB_i is the uncertainty in each basin's SMB.

3. Results

3.1. Changes in Ice Velocity and Ice Discharge from 2000 to 2020

We obtained ice velocity change (Figure 3) and ice discharge results change (Figure 4) for 2000, 2007–2011, 2013–2017, and 2017–2020. The AIS was further divided into six sea sectors to better demonstrate the spatial and temporal characteristics of ice velocity and ice discharge changes over the past 20 years.

Overall, our results show that the ice discharge has been increasing over time for the whole Antarctic in the four periods, with values of 1792 ± 47 Gt/yr, 1876 ± 51 Gt/yr, 1908 ± 51 Gt/yr, and 1940 ± 37 Gt/yr for the periods 2000, 2007–2011, 2013–2017, and 2017–2020, respectively (Table 2). The Amundsen Sea sector contributes ~70% of the discharge growth between the 2000 and 2017–2020 periods and is the region with the most rapidly increasing ice discharge in Antarctica (Figure 3). In addition, both the WAIS and the EAIS show increasing trends in ice discharge during the study period. From 2000 to 2017–2020, the discharge from the WAIS grew from 652 ± 32 Gt/yr to 753 ± 29 Gt/yr, an increase of up to 15%, and the discharge from the EAIS grew from 968 ± 32 Gt/yr to 1000 ± 22 Gt/yr. The growth rates of ice discharge vary from region to region over time. Below, we divided the AIS into six sectors to demonstrate the changes in detail.

Table 2. The area of the 27 basins, ice discharge for the periods of 2000, 2007–2011, 2013–2017, and 2017–2020, and the mean SMB for the study years.

Basin	Area (km ²)	Discharge (Gt/yr)				Mean of SMB (Gt/yr)
		2000	2007–2011	2013–2017	2017–2020	
1	479,840	114 ± 25	115 ± 20	115 ± 20	120 ± 7	133 ± 27
2	780,488	50 ± 3	49 ± 8	49 ± 4	50 ± 4	55 ± 11
3	1,570,432	65 ± 8	66 ± 5	67 ± 4	66 ± 2	75 ± 15
4	244,696	40 ± 8	43 ± 9	43 ± 10	43 ± 5	48 ± 10
5	186,884	31 ± 4	35 ± 5	34 ± 7	35 ± 3	35 ± 7
6	606,040	59 ± 8	58 ± 12	57 ± 13	58 ± 6	70 ± 14
7	493,857	57 ± 9	63 ± 12	63 ± 11	67 ± 8	88 ± 18
8	159,829	21 ± 5	23 ± 8	22 ± 5	22 ± 3	35 ± 7
9	145,674	16 ± 4	18 ± 6	17 ± 3	17 ± 2	18 ± 4
10	919,362	43 ± 2	43 ± 2	42 ± 2	42 ± 1	40 ± 8
11	257,477	15 ± 3	14 ± 6	14 ± 3	14 ± 1	15 ± 3
12	719,472	114 ± 14	119 ± 18	124 ± 15	124 ± 11	121 ± 24
13	1,109,722	208 ± 14	212 ± 18	218 ± 19	216 ± 16	191 ± 38
14	711,661	127 ± 11	128 ± 16	134 ± 15	133 ± 14	129 ± 26
15	124,081	31 ± 7	26 ± 7	30 ± 6	30 ± 6	28 ± 6
16	265,501	16 ± 3	15 ± 3	14 ± 2	15 ± 1	12 ± 2

Table 2. Cont.

Basin	Area (km ²)	Discharge (Gt/yr)				Mean of SMB (Gt/yr)
		2000	2007–2011	2013–2017	2017–2020	
17	1,843,824	78 ± 11	71 ± 14	63 ± 13	68 ± 9	82 ± 16
18	266,471	11 ± 1	11 ± 2	9 ± 2	10 ± 1	29 ± 6
19	372,696	48 ± 4	47 ± 6	47 ± 4	47 ± 3	44 ± 9
20	182,833	148 ± 15	148 ± 10	168 ± 17	170 ± 15	124 ± 25
21	210,994	155 ± 10	175 ± 10	183 ± 11	192 ± 11	106 ± 21
22	213,744	98 ± 4	131 ± 3	131 ± 4	139 ± 3	87 ± 17
23	75,159	78 ± 8	80 ± 6	77 ± 10	75 ± 8	73 ± 15
24	100,865	83 ± 8	85 ± 5	88 ± 7	88 ± 6	90 ± 18
25	34,212	48 ± 7	61 ± 8	60 ± 9	59 ± 8	71 ± 14
26	41,519	28 ± 4	30 ± 3	27 ± 4	28 ± 3	44 ± 9
27	52,136	13 ± 3	12 ± 1	12 ± 2	12 ± 1	21 ± 4
EAIS	10,139,000	968 ± 32	980 ± 26	991 ± 31	1000 ± 22	1042 ± 64
WAIS	1,801,737	652 ± 32	707 ± 42	730 ± 39	753 ± 29	596 ± 49
AP	228,732	172 ± 12	188 ± 10	187 ± 12	187 ± 10	226 ± 25
Total	12,169,469	1792 ± 47	1876 ± 51	1908 ± 51	1940 ± 37	1864 ± 85

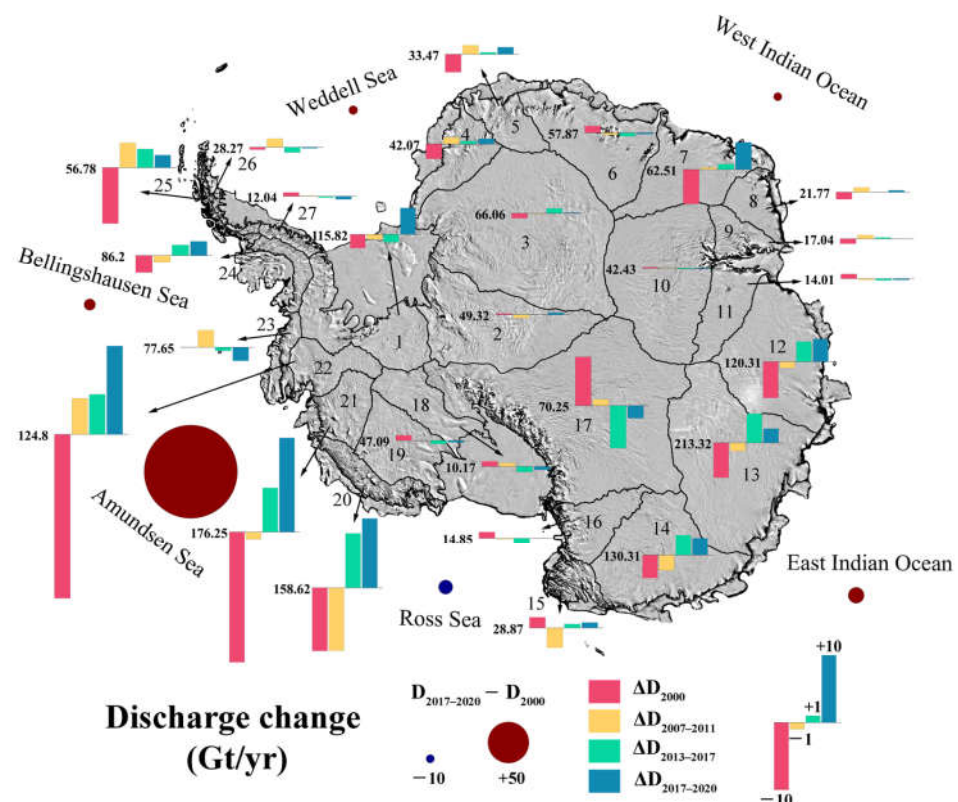


Figure 3. Ice discharge changes in different sea sectors and different basins. The bar charts show the anomaly from the mean value (left side of the bar chart) for different periods (shown in different colors). The circles show the discharge changes for different sea sectors between 2017–2020 and 2000. The bar length and the circle size are proportional to the absolute magnitude of the change in discharge. The circle colors represent the negative (blue) or positive (red) state. The base map is the MODIS mosaic of Antarctica [41], and the black lines are the basin boundaries [29].

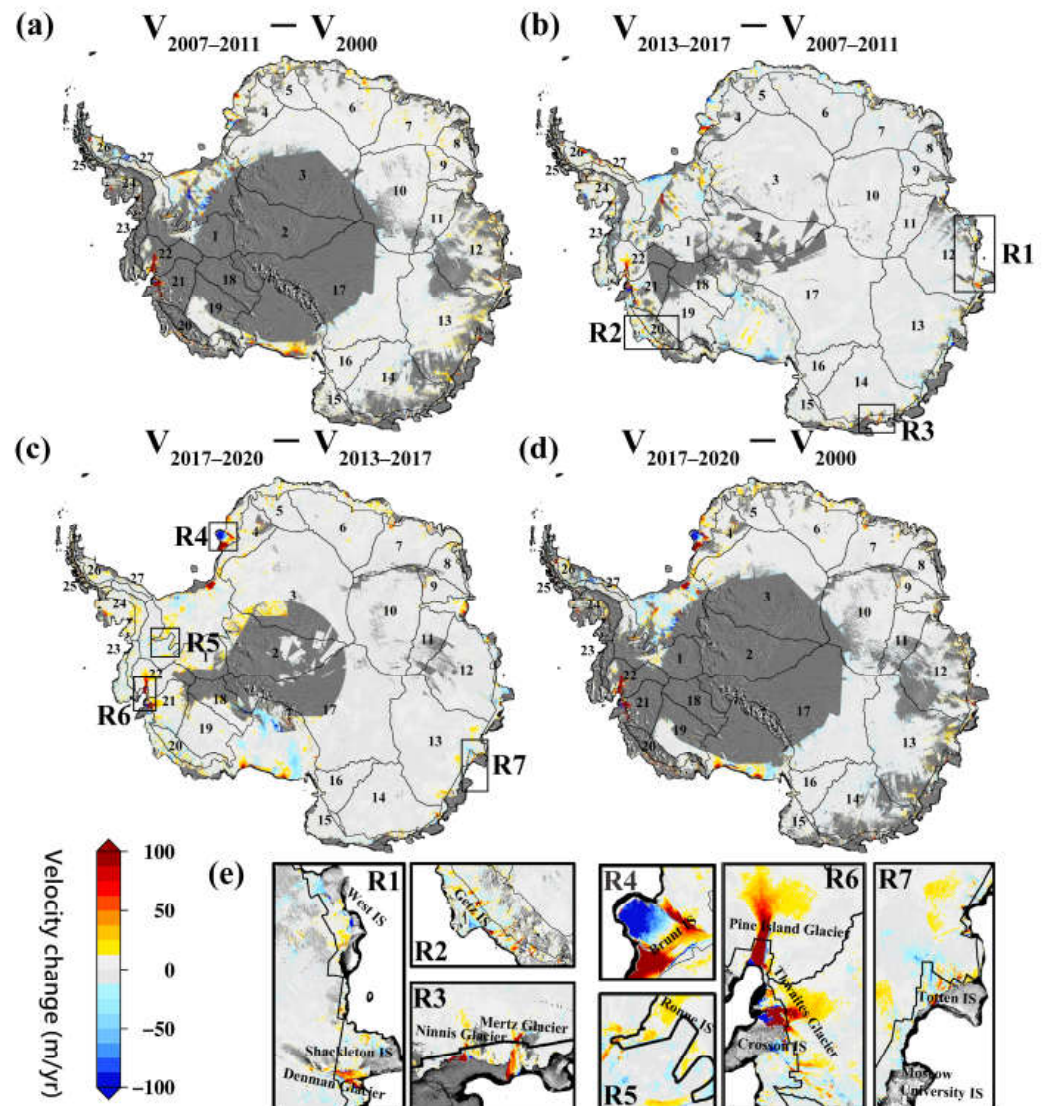


Figure 4. Antarctic-wide ice velocity changes in four different periods: (a) from 2000 to 2007–2011; (b) from 2007–2011 to 2013–2017; (c) from 2013–2017 to 2017–2020; (d) from 2000 to 2017–2020. The black rectangles show the locations of R1–R7 in (e). The black line is the basin boundary produced with the flux gate. (e) Seven regions (R1–R7) with significant changes.

3.1.1. Amundsen Sea Sector (B20–B22)

Our results show that the Amundsen Sea sector is the region with the most dramatic increase in Antarctic ice velocity and ice discharge, as previous studies have revealed [8,17]. The ice discharge in this sector was approximately 114 Gt/yr higher in 2017–2020 than in 2000, which is approximately ten times the change in other sea sectors. The enormous ice velocity change in B20 occurred at the Getz Ice Shelf (Getz IS). The ice velocity at the FG in this region increased up to 300 m/yr between 2000 and 2017–2020. The ice discharge in B20 increased by 22 Gt/yr during this period, with most of the discharge increases occurring between 2007–2011 and 2013–2017 due to significant ice velocity increases (R2 in Figure 4e).

The more representative region of B21 is the Thwaites Glacier, Smith Glacier, and Pope Glacier, which showed an average increase in ice velocity from 2000 to 2017–2020 of 83 m/yr. The ice velocity along the Thwaites Glacier FG increased by an average of 213 m/yr to a maximum of 1137 m/yr. The ice discharge in B21 increased ~20% from 2017–2020 compared with 2000. The ice velocity and discharge in this region showed a consistent increase in each period.

The main outlet glacier in B22 is Pine Island Glacier, one of the fastest-flowing glaciers in Antarctica. Between 2000 and 2017–2020, the average ice velocity increased by 365 m/yr at the FG of this glacier. The ice discharge in B22 increased by 41.1 Gt/yr, i.e., ~40%, the largest increase among all the basins in Antarctica. However, the ice discharge remained stable between 2007–2011 and 2013–2017 (Figure 3). This is similar to the conclusion of Rignot et al. [8], that the mass loss of the Pine Island Glacier stabilized after 2012. However, this glacier's surface ice velocity increased again between 2013–2017 and 2017–2020 (R6 in Figure 4e). The ice velocity reached a maximum of just over 4 km/year, significantly increasing the mass loss from Pine Island Glacier.

3.1.2. Bellingshausen Sea Sector (B23–B25)

The overall trend of ice discharge growth in the Bellingshausen Sea sector was 13.7 Gt/yr from 2000 to 2017–2020. The largest contribution was 11.1 Gt/yr from B25, with a significant discharge increase found between 2000 and 2007–2011. The ice discharge in B24 maintained a slow growth trend during the study period, while the discharge in B23 exhibited almost no change and was relatively stable. The ice discharge for all the basins in this sector remained stable in the period from 2013–2017 to 2017–2020.

3.1.3. Weddell Sea Sector (B26, B27, and B1–B5)

There was a slight increase in ice discharge in the Weddell Sea sector during the study period, with an increase of approximately 10.6 Gt/yr from 2000 to 2017–2020. For B4 and B5 in this sector, the discharge changes mainly occurred before 2011. It is worth noting the significant increase in ice discharge in B1 between 2013–2017 and 2017–2020. The ice velocity in this basin also increased during this period (R5 in Figure 4e). The maximum velocity increases reached 97 m/yr in some regions. In addition, the Brunt Ice Shelf (Brunt IS) experienced a dramatic change in ice velocity (R4 in Figure 4e), as other studies have also revealed [42].

3.1.4. West Indian Ocean Sector (B6–B11)

During the study period, there was a weak increase in ice discharge in this sector, with a value of only approximately 9.9 Gt/yr. This increase was mainly due to the increase in ice discharge from B7, while the discharge of other basins remained stable during the study period. We also found that the ice velocity increased by a up to ~200 m/yr in some regions of B7.

3.1.5. East Indian Ocean Sector (B12–B14)

The increase in ice discharge in this sector between 2000 and 2017–2020 was approximately 18.9 Gt/yr. This increase mainly occurred between 2000 and 2013–2017, while the total ice discharge stopped increasing from 2013–2017 to 2017–2020.

The ice velocity along the FG in B13 showed an obvious increase between 2000 and 2007–2011, with the most significant increase occurring in the Vincennes Bay region with an average of 55 m/yr. As with the overall discharge changes in this sector, the ice discharge of B13 showed a slight decrease between 2013–2017 and 2017–2020, mainly resulting from the decrease in ice velocity of the two main glaciers in this basin. The ice velocity of Totten Glacier decreased by an average of 11 m/yr during this period, and that of Moscow University Glacier also showed a slight decline (R7 in Figure 4e).

In B12, the glaciers feeding the West Ice Shelf (West IS) and the Shackleton Ice Shelf (Shackleton IS) showed an average increase in ice velocity of approximately 17 m/yr, reaching up to 450 m/yr in some regions from 2000 to 2007–2011. Although glaciers feeding the West IS showed a deceleration from 2007–2011 to 2013–2017, the ice velocity of glaciers feeding the Shackleton IS continued to increase during this period (R1 in Figure 4e). There was a slight decrease in the ice velocity of glaciers feeding the West IS and the Shackleton IS from 2013–2017 to 2017–2020, similar to the trend of B13. The ice velocity of the Ninnis Glacier and the Mertz Glacier in B14 rapidly increased from 2007–2011 to

2013–2017 (R3 in Figure 4e), resulting in an ice discharge increase of ~6 Gt/yr during this period. However, again, the ice velocity remained almost unchanged between 2013–2017 and 2017–2020.

3.1.6. Ross Sea Sector (B15–B19)

The Ross Sea sector is the only region where ice discharge decreased during the study period, with a reduction of 17.0 Gt/yr from 2000 to 2017–2020. This is most likely due to the ice velocity decrease in B17 and B18. For the recent period from 2013–2017 to 2017–2020, the average annual ice discharge slightly increased by 7.0 Gt/yr.

3.2. SMB Calculation and Changes

We first performed a correlation test to demonstrate the similarity of the SMB results estimated from ERA5-Land and RACMO2.3 at the annual scale (Figure 5). In the EAIS, we used the SMB results of RACMO2.3p1 and ERA5-Land from 1979–2015 for the test, and they showed a strong correlation. The R^2 is as high as 0.755 (Figure 5a), and the slope of the linear fit trend line is 0.924. In the WAIS and the AP, we used the results of RACMO2.3p2 and ERA5-Land from 1979–2017. The data for the WAIS and the AP also showed strong correlations over these 39 years, with R^2 values of 0.877 (Figure 5b) and 0.929 (Figure 5c), respectively. In summary, ERA5-Land reanalysis results strongly correlated with the RACMO2.3 SMB outputs and could be used to extend the RACMO2.3 SMB results.

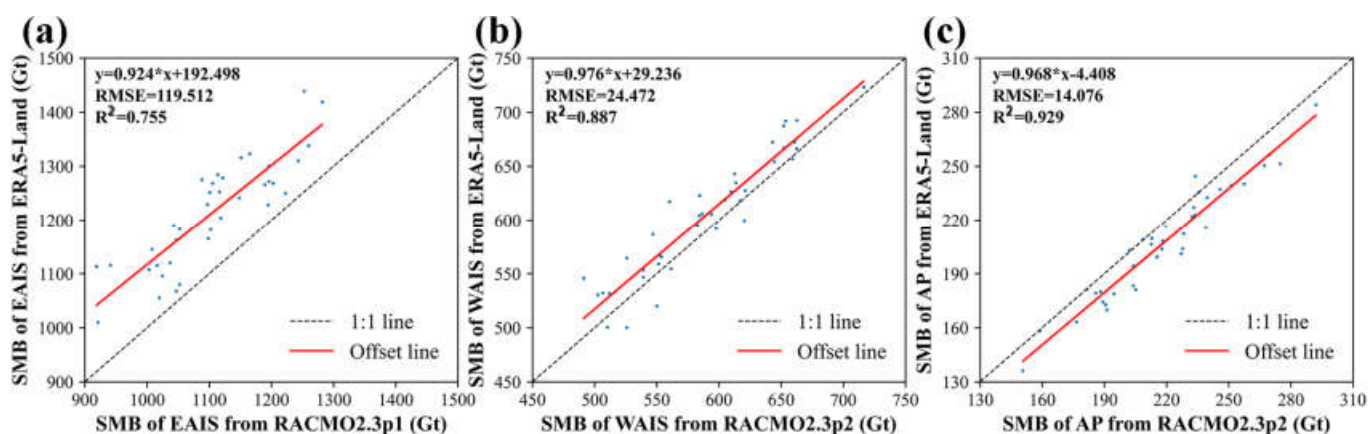


Figure 5. Comparison of annual SMB estimated from ERA5-Land and RACMO2.3 output. (a) The SMB of ERA5-Land against the SMB from RACMO2.3p1 in the EAIS from 1979 to 2015. (b) The SMB of ERA5-Land against the SMB from RACMO2.3p2 in the WAIS from 1979 to 2017. (c) The SMB of ERA5-Land against the SMB from RACMO2.3p2 in the AP from 1979 to 2017.

Using the method described in Section 2.4, we extended the RACMO2.3 SMB records to 2020 (Figure 6). The annual SMB results for all of Antarctica during the study period 2000–2020 range between 1694–2104 Gt, with a maximum interannual difference of up to 410 Gt. The interannual changes in the SMB for the EAIS, WAIS, and AP range from 994–1280 Gt, 486–687 Gt, and 159–292 Gt, respectively. The large interannual fluctuations in the SMB may directly contribute to the interannual change in the mass balance. However, the Antarctic SMB does not show a significant trend during our study period [43].

3.3. Changes in the Mass Balance

The mean value of the AIS mass balance for 2000–2020 was -89 ± 99 Gt/yr (Table 3). During the study period, almost all the years show a state of mass loss. This generally agrees with recent estimates of Antarctic mass change based on laser altimetry of -118 ± 24 Gt/yr for 2003–2019.

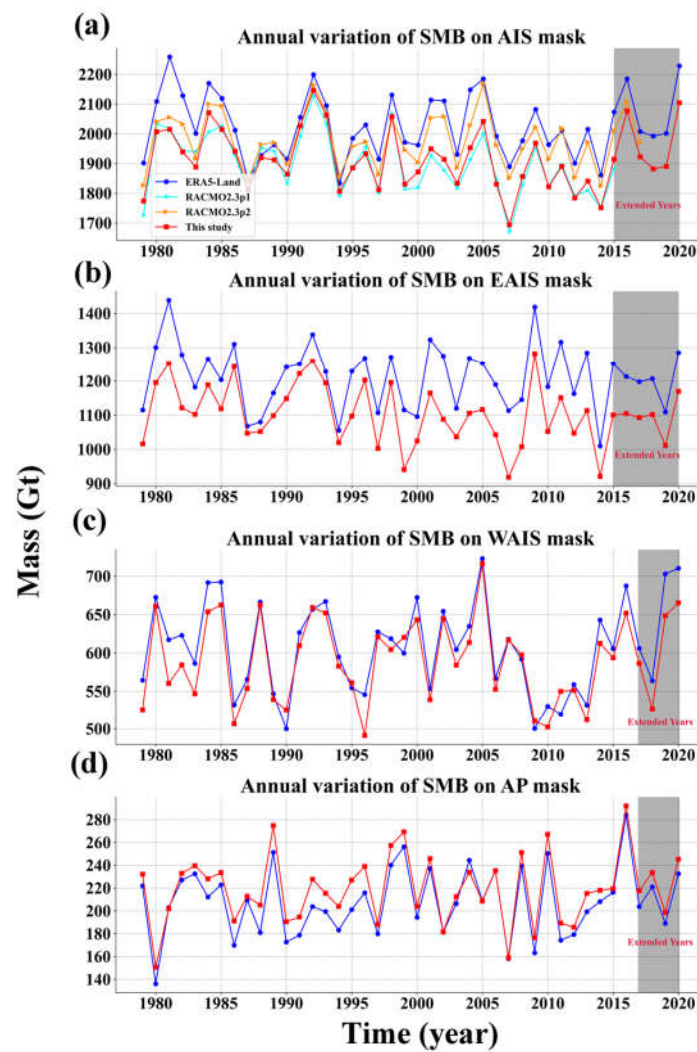


Figure 6. Comparison of annual SMB estimated from ERA5-Land and RACMO2.3 output. (a) The SMB of ERA5-Land against the SMB from RACMO2.3 in the AIS. (b) The SMB of ERA5-Land against the SMB from RACMO2.3p1 in the EAIS. (c) The SMB of ERA5-Land against the SMB from RACMO2.3p2 in the WAIS. (d) The SMB of ERA5-Land against the SMB from RACMO2.3p2 in the AP.

Table 3. Mass balance in the four periods 2000, 2007–2011, 2013–2017, and 2017–2020 for the 27 basins.

Basin	Mass Balance (Gt/yr)				Mean
	2000	2007–2011	2013–2017	2017–2020	
1	13 ± 36	15 ± 33	21 ± 34	14 ± 28	17 ± 32
2	3 ± 11	4 ± 13	7 ± 12	8 ± 12	6 ± 12
3	11 ± 17	6 ± 15	10 ± 16	11 ± 16	9 ± 16
4	1 ± 11	5 ± 13	4 ± 14	9 ± 12	5 ± 13
5	−1 ± 7	−3 ± 8	4 ± 10	3 ± 8	1 ± 9
6	13 ± 17	3 ± 17	18 ± 20	13 ± 15	12 ± 18
7	20 ± 18	20 ± 21	23 ± 21	31 ± 21	24 ± 21
8	9 ± 8	11 ± 10	13 ± 9	16 ± 9	13 ± 9
9	−3 ± 4	0 ± 7	0 ± 5	2 ± 4	1 ± 6
10	−7 ± 7	0 ± 9	−5 ± 8	−2 ± 8	−2 ± 8
11	−1 ± 4	1 ± 6	1 ± 5	1 ± 3	1 ± 5
12	3 ± 28	14 ± 32	−6 ± 29	−12 ± 25	−1 ± 28
13	12 ± 46	−27 ± 41	−18 ± 44	−40 ± 39	−24 ± 42
14	−14 ± 25	−20 ± 27	10 ± 32	5 ± 31	−2 ± 30

Table 3. Cont.

Basin	Mass Balance (Gt/yr)				Mean
	2000	2007–2011	2013–2017	2017–2020	
15	0 ± 9	−2 ± 8	0 ± 9	−1 ± 8	−1 ± 8
16	−2 ± 4	−4 ± 4	−4 ± 3	0 ± 3	−3 ± 3
17	12 ± 21	5 ± 21	13 ± 20	25 ± 21	14 ± 20
18	17 ± 6	15 ± 6	21 ± 7	21 ± 6	19 ± 6
19	−5 ± 9	−7 ± 10	−1 ± 10	−1 ± 10	−3 ± 10
20	−13 ± 31	−37 ± 26	−44 ± 30	−38 ± 30	−37 ± 29
21	−28 ± 27	−74 ± 23	−82 ± 23	−81 ± 25	−75 ± 24
22	4 ± 21	−45 ± 17	−46 ± 18	−53 ± 18	−43 ± 17
23	3 ± 18	−2 ± 17	−7 ± 17	−7 ± 16	−5 ± 17
24	3 ± 19	4 ± 19	9 ± 21	−7 ± 17	3 ± 19
25 *	−10 ± 13	−10 ± 13	−10 ± 13	−10 ± 13	−10 ± 13
26 *	−16 ± 10	−16 ± 10	−16 ± 10	−16 ± 10	−16 ± 10
27	8 ± 5	7 ± 4	10 ± 5	9 ± 4	9 ± 4
EAIS	56 ± 62	13 ± 55	70 ± 58	70 ± 55	53 ± 56
WAIS	−9 ± 73	−135 ± 75	−137 ± 77	−145 ± 71	−127 ± 74
AP	−15 ± 25	−15 ± 28	−7 ± 29	−24 ± 26	−15 ± 32
AIS	33 ± 99	−137 ± 97	−75 ± 101	−99 ± 93	−89 ± 99

* The final mass balance for the northern AP (B25 and B26) is determined by the mass balance estimate of the altimetric method [7].

The mass balance of the EAIS during the study period was positive, which agrees well with most estimates for the EAIS [4,10,17]. The average mass accumulation of the EAIS from 2000 to 2020 was 53 ± 74 Gt/yr, and the average mass accumulation values in 2000, 2007–2011, 2013–2017, and 2017–2020 were 56 ± 62 Gt/yr, 13 ± 55 Gt/yr, 70 ± 58 Gt/yr, and 70 ± 55 Gt/yr, respectively (Table 3). The anomalously low SMB value in approximately 2007 led to a smaller mass balance in 2007–2011 than in other years. The basins with significant mass growth were B6–B8 (Queen Mary Land) and B17, which contributed 63 ± 34 Gt/yr to the mass accumulation of the EAIS. The mass of the Amery Ice Shelf region (B9–B11) was nearly balanced during the entire study period, which is consistent with most studies of the region within the stated errors (Table 3) [21,39]. In contrast, the East Indian Ocean sector (B12–B14) showed a significant acceleration in mass loss between 2000 and 2017–2020, which deserves more attention. The mass balance in this region changed from a weak mass equilibrium (1 ± 59 Gt/yr) in 2000 to a state of dramatic mass loss ($−47 \pm 55$ Gt/yr) in 2017–2020. Considering that the ice discharge in this sector was almost unchanged between 2013–2017 and 2017–2020, the recent acceleration in mass loss was likely mainly associated with the decline in the SMB in the region in 2017–2020.

The WAIS is the region with the most severe mass loss, with a mean mass balance of $−127 \pm 56$ Gt/yr (Table 3) over the period 2000–2020. In particular, the Amundsen Sea sector (B20–B22), which has undergone multiple ice shelf breakups and continued ice shelf thinning [44,45], had a mean mass loss of $−155 \pm 24$ Gt/yr during the study period. The mass loss showed an acceleration between 2000 and 2013–2017, which is most likely attributable to the rapid increase in ice discharge in the Getz, Pine Island, Thwaites, and Crosson areas in this region (Figure 3). The WAIS maintained a high state of mass loss in 2017–2020 with no indication of slowing down, suggesting that this region will need continued monitoring.

4. Discussion

4.1. Comparison with Other Estimates

In order to evaluate the differences of mass balance assessments utilizing different methods, we conducted a comparative analysis of our estimates against those results from the gravity-based method, the altimetry-based method, and other IOM-based estimates (Table 4).

Table 4. Results of mass balance from our IOM-based estimate, the gravity-based method, and the altimetry-based method.

Method	Region	Span (Years)	Mean of Mass Balance (Gt/yr)	Uncertainty (Gt/yr)
IOM	EAIS	2013–2020	70	66
	WAIS	2013–2020	−141	61
	AP	2013–2020	−14	24
	AIS	2013–2020	−85	93
Gravimetry	EAIS	2013–2020	50	/
	WAIS	2013–2020	−118	/
	AP	2013–2020	−13	/
	AIS	2013–2020	−81	/
Altimetry *	EAIS	2003–2019	90	21
	WAIS	2003–2019	−169	10
	AP	2003–2019	−39	5
	AIS	2003–2019	−118	24

* Note that the values are calculated combining our ice cover boundary as a mask with the dm/dt results provided by Smith et al. [7].

4.1.1. Comparison with Gravimetry-Derived Mass Change

We compared the results from our assessment with the mass balance calculated from gravimetry measurements spanning the years 2013–2020 [10]. We constructed a time series of mass balance data for the AIS from both our results and those obtained through the gravity calculations. During the 2013–2020 period, our estimated AIS mass loss was 595 Gt, while gravity results indicated a mass loss of 567 Gt for the period January 2013–September 2019 (Figure 7a). The results obtained through these two methods were found to be in close agreement. In the EAIS, both our results and the gravity inversions indicate that the EAIS was slowly gaining mass. However, our calculated mass increase (489 Gt) appears to be larger than the gravity results (419 Gt), which we speculate is due to basal melting of the ice sheet, as reported in [46]. Previous study has shown that the total basal mass balance over AIS decreased at an average rate of 21 ± 22 Gt/yr from 2003 to 2009, about twice as much mass change as the discrepancy observed in the EAIS. Although the time periods differ, the magnitude of annual total basal mass loss suggests that ice sheet basal melting is non-negligible, particularly when calculating the mass budget using IOM. In addition, recent study has indicated that current models significantly underestimate the basal melting rate in Antarctica [47], providing strong support for our speculation. The WAIS is the region that shows the best agreement between our results and the gravity results (Figure 7c). The AP also exhibits similar trends in our data and the gravity results (Figure 7d). Although the monthly estimates from gravity inversion contain more detail than our annual estimates, the results of the two methods agree well.

4.1.2. Comparison with Altimetry-Derived Mass Change

We conducted a comparison of our results with recent altimetry-based mass balance estimates of the AIS [7]. The altimetry-based results indicate that the mass change rate for the AIS, EAIS, WAIS, and AP between 2003 and 2019 was -118 ± 24 Gt/yr, 90 ± 21 Gt/yr, -169 ± 10 Gt/yr, and -39 ± 5 Gt/yr, respectively. Our estimates were found to be consistent with those of Smith et al. [7] within stated errors. Both results reveal mass gains in the EAIS and significant ice loss in the WAIS. However, the altimetry-based mass balance estimates were found to be more positive for the EAIS and more negative for the WAIS. We speculate that these differences are mainly due to the variations in the area of investigation. Our estimates were solely focused on the grounded ice sheet region, while

the altimetry-based estimates also included peripheral islands. To enable a comparison of the two results on the same continental extent, we used our ice sheet boundary to mask the dm/dt results provided by Smith et al. [7]. Subsequently, the altimetry-based mass balance of the AIS, EAIS, WAIS, and AP were found to be -89 ± 24 Gt/yr, 89 ± 21 Gt/yr, -146 ± 10 Gt/yr, and -32 ± 5 Gt/yr, respectively. Considering the slight differences in the study period, our results agree quite well with the altimetry-based estimates.

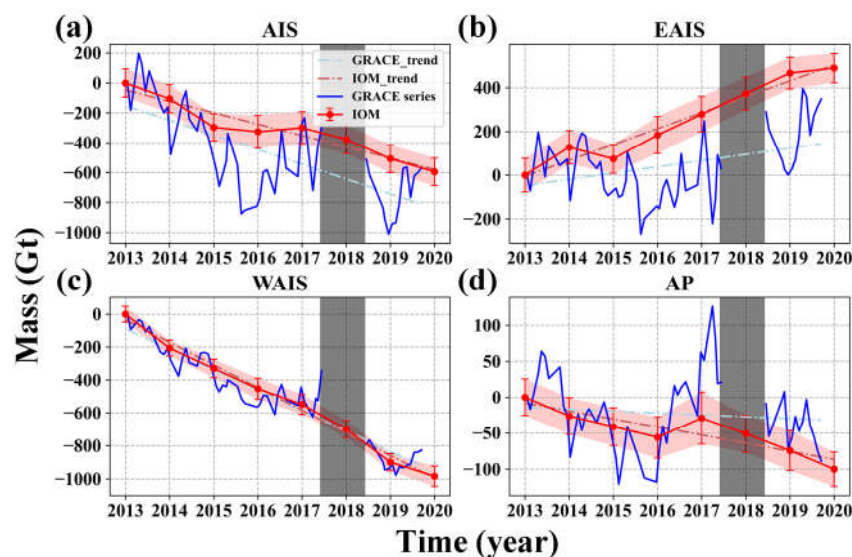


Figure 7. Comparison of our mass balance estimates with Gravity Recovery and Climate Experiment (GRACE) and GRACE Follow-On (FO) mass change estimates for 2013–2020 in (a) the AIS, (b) the EAIS, (c) the WAIS, and (d) the AP [10]. The red shaded part in the figure represents the uncertainty range of our calculation, and the red dashed line and light blue dotted line represent the trends of our study’s results and the gravity-based results from 2013 to 2020, respectively. Gray vertical bar indicates the gap between the end of GRACE and the start of GRACE-FO.

4.1.3. Comparison with Other IOM-Based Results

The results derived from different IOM schemes have been found to exhibit substantial variation, primarily due to the different designs of the experiment, as reflected in the calculation of ice discharge. Our estimate of ice discharge of 1908 ± 51 Gt/yr during the 2013–2017 period differs from other estimates. The ice discharge values of the AIS estimated by Gardner et al. [16], Shen et al. [17], and Rignot et al. [8] were 1929 ± 40 Gt/yr (2015), 2136 ± 42 Gt/yr (2014–2015), and 2311 ± 142 Gt/yr (2013–2017), respectively. Our results were in good agreement with Gardner et al. [16], which may be due to the fact that we both estimated the AIS mass balance using a similar flux gate. On the other hand, differences in ice thickness data may be responsible for the discrepancy between our results and those reported by Shen et al. [17] and Rignot et al. [8]. Shen et al. [17] and Rignot et al. [8] primarily utilized data from Bedmap-2 [1] and Operation Ice Bridge, while we estimated the ice thickness from BedMachine. We speculate that the differences in the method and data used may have led to the discrepancy between different IOM studies.

Furthermore, it should be noted that the ice velocity products used in this study differ from previous studies. Thus, we carry out an analysis of the regional ice velocity differences from previous studies to determine if any variation observed are real or mere artifacts. In the EAIS, we note a continuous slight decrease in ice velocity from 2007–2011 to 2017–2020 on the Totten Glacier, which is distinct from the velocity increase recorded during the period of 2000–2007, as reported in a previous study [18]. This reduction in ice velocity has also been observed by Miles et al. [48], and is thought to result from intermittent contact between the ice shelf and bed obstacles. Note that an unusual increase in velocity at the north edge of Law Dome was observed in our results. We speculate this is just artifacts and not a real velocity variation. Furthermore, these artefacts have no impact on our ice

discharge estimate as they are located far from the flux gate. On Ninnis Glacier and Mertz Glacier, we found acceleration mainly occurred at the floating ice shelves from 2007–2011 to 2017–2020, which was consistent with the results from Rignot et al. [28]. Additionally, a study of the calving cycle of the Ninnis Glacier found that its acceleration was closely related to the calving event and that the velocity at the grounding line was almost constant from 2013–2019 [49], which aligned with the results obtained in this study. Overall, the results on ice velocity changes in this study were consistent with most previous studies at the regional scale, although some velocity artifacts were present in the velocity products with little impact on the calculation of ice discharge.

4.2. Most Recent Changes

The WAIS exhibits pronounced changes in ice discharge, with an increase from 652 Gt/yr of the earlier 2000 period to 753 Gt/yr of the recent 2017–2020 period. About 70% of the discharge growth is attributed to the glacier speedup in the Amundsen Sea sector. As the region exhibiting the most dramatic changes, the Amundsen Sea sector merits further examination. The current ice velocity in the region has been found to be dramatically increasing (Figure 3), the ice thickness is decreasing (Figure 2), the rate of ice discharge is significantly increasing over time (Table 2), and the mass loss is significant (Table 3). The dramatic changes observed in this sector can be attributed to several factors. The primary cause is believed to be the wind-driven incursion of warm, salty, Circumpolar Deep Water (CDW) beneath the ice shelf [50], which leads to increased ice shelf basal melt rates and resultant changes in ice shelf buttressing [51,52]. In addition, the intrusion of maritime air masses over the ice sheet may result in extensive melt events [53].

B12–B14 in the East Indian Ocean sector have been identified as notable areas where numerous studies have reported mass losses [18,38]. Our study also found that this region exhibited a negative mass balance. In the period 2017–2020, we observed a slight decrease in ice velocity and a cessation of the continuous increase in ice discharge, as previously reported in another study [48]. However, the mass loss in this region remained higher than it was in the period 2013–2017 (Table 3), which suggests that a decrease in discharge alone is unlikely to have changed the state of the mass balance. The relatively low mass loss observed in 2013–2017 may have been related to the extreme El Niño that occurred during 2015–2016, which altered moisture transport patterns and resulted in increased precipitation in the coastal area [54]. The reasons for the decrease in the ice velocity in this region warrant further investigation.

5. Conclusions

In this study, we estimated the mass balance of the AIS for the period 2000 to 2020 using the IOM. We used interannual-scale Antarctic-wide ice velocity and state-of-the-art AIS thickness datasets and extended RACMO2.3 SMB records. We found that the overall discharge in the AIS showed an increasing trend, with the discharges in 2000, 2007–2011, 2013–2017, and 2017–2020 being 1792 ± 47 Gt/yr, 1876 ± 51 Gt/yr, 1908 ± 51 Gt/yr, and 1940 ± 37 Gt/yr, respectively. The discharge of the WAIS increased three to four times more than that of the EAIS in the same period. The Amundsen Sea sector was the most significant contributor to the increase in ice discharge. Additionally, for the East Indian Ocean sector (B12–B14), we found a slight decrease in ice discharge during 2017–2020 instead of a continuation of the upward trend of the previous period. The mass balance of the AIS was in a state of mass loss in the early 21st Century, with a mean value of -89 ± 99 Gt/yr over the study period. The EAIS showed a slightly positive mass balance, with some basins in the East Indian Ocean (B12–B14) showing mass losses. The mass loss in the WAIS was significant, accounting for approximately 70% of the total Antarctic mass loss and exhibiting a dramatic increasing trend. Furthermore, our mass balance estimates agreed with gravity inversion and altimetry-based results. In general, the discharges of the AIS have continued to grow in recent years (Figure 3). The discharge of B22 in the Amundsen Sea sector seems to have stopped growing between 2007–2011 and 2013–2017,

but then increased again during 2017–2020. The East Indian Ocean sector (B12–B14) showed a decreased discharge during 2017–2020 (Table 2). The mass balance in 2017–2020 was -99 ± 93 Gt/yr, slightly above the average value of the study period.

Author Contributions: Conceptualization, Q.L.; methodology, Q.L. and T.Y.; software, T.Y.; validation, T.Y.; formal analysis, Q.L. and T.Y.; investigation, Q.L. and T.Y.; resources, X.C.; data curation, T.Y.; writing—original draft preparation, T.Y.; writing—review and editing, Z.C., F.H., X.C., T.L., L.Z. and Q.L.; visualization, T.Y.; supervision, Q.L.; project administration, Q.L.; funding acquisition, X.C. All authors have read and agreed to the published version of the manuscript.

Funding: This research was supported by the National Natural Science Foundation of China (grant no. 42006192), Guangdong Basic and Applied Basic Research Foundation (2023A1515010925), and the Innovation Group Project of Southern Marine Science and Engineering Guangdong Laboratory (Zhuhai) (grant no. 311021008).

Data Availability Statement: Multiple ice velocity datasets, ice thickness, grounding lines, flux gates and basin boundary are available from the National Snow and Ice Data Center (NSIDC). The ERA5-Land are available from the European Centre for Medium-Range Weather Forecasts (ECMWF).

Acknowledgments: The authors thank the NSIDC for providing datasets. The authors thank the ECMWF for providing reanalysis product. The authors also thank J. M. van Wessem for providing the RACMO 2.3p1/p2 dataset.

Conflicts of Interest: The authors declare no conflict of interest.

References

1. Fretwell, P.; Pritchard, H.D.; Vaughan, D.G.; Bamber, J.L.; Barrand, N.E.; Bell, R.; Bianchi, C.; Bingham, R.G.; Blankenship, D.D.; Casassa, G.; et al. Bedmap2: Improved Ice Bed, Surface and Thickness Datasets for Antarctica. *Cryosphere* **2013**, *7*, 375–393. [[CrossRef](#)]
2. Bamber, J.L.; Westaway, R.M.; Marzeion, B.; Wouters, B. The Land Ice Contribution to Sea Level during the Satellite Era. *Environ. Res. Lett.* **2018**, *13*, 063008. [[CrossRef](#)]
3. Morlighem, M.; Rignot, E.; Binder, T.; Blankenship, D.; Drews, R.; Eagles, G.; Eisen, O.; Ferraccioli, F.; Forsberg, R.; Fretwell, P.; et al. Deep Glacial Troughs and Stabilizing Ridges Unveiled beneath the Margins of the Antarctic Ice Sheet. *Nat. Geosci.* **2020**, *13*, 132–137. [[CrossRef](#)]
4. The IMBIE team Mass Balance of the Antarctic Ice Sheet from 1992 to 2017. *Nature* **2018**, *558*, 219–222. [[CrossRef](#)]
5. Thomas, E.R.; van Wessem, J.M.; Roberts, J.; Isaksson, E.; Schlosser, E.; Fudge, T.J.; Vallelonga, P.; Medley, B.; Lenaerts, J.; Bertler, N.; et al. Regional Antarctic Snow Accumulation over the Past 1000 Years. *Clim. Past* **2017**, *13*, 1491–1513. [[CrossRef](#)]
6. Wadhwa, J.L.; Hawkings, J.R.; Tarasov, L.; Gregoire, L.J.; Spencer, R.G.M.; Gutjahr, M.; Ridgwell, A.; Kohfeld, K.E. Ice Sheets Matter for the Global Carbon Cycle. *Nat. Commun.* **2019**, *10*, 3567. [[CrossRef](#)]
7. Smith, B.; Fricker, H.A.; Gardner, A.S.; Medley, B.; Nilsson, J.; Paolo, F.S.; Holschuh, N.; Adusumilli, S.; Brunt, K.; Csatho, B.; et al. Pervasive Ice Sheet Mass Loss Reflects Competing Ocean and Atmosphere Processes. *Science* **2020**, *368*, 1239–1242. [[CrossRef](#)] [[PubMed](#)]
8. Rignot, E.; Mouginot, J.; Scheuchl, B.; van den Broeke, M.; van Wessem, M.J.; Morlighem, M. Four Decades of Antarctic Ice Sheet Mass Balance from 1979–2017. *Proc. Natl. Acad. Sci. USA* **2019**, *116*, 1095–1103. [[CrossRef](#)] [[PubMed](#)]
9. Schröder, L.; Horwath, M.; Dietrich, R.; Helm, V.; van den Broeke, M.R.; Ligtenberg, S.R.M. Four Decades of Antarctic Surface Elevation Changes from Multi-Mission Satellite Altimetry. *Cryosphere* **2019**, *13*, 427–449. [[CrossRef](#)]
10. Velicogna, I.; Mohajerani, Y.; Landerer, F.; Mouginot, J.; Noel, B.; Rignot, E.; Sutterley, T.; Broeke, M.; Wessem, M.; Wiese, D. Continuity of Ice Sheet Mass Loss in Greenland and Antarctica From the GRACE and GRACE Follow-On Missions. *Geophys. Res. Lett.* **2020**, *47*, e2020GL087291. [[CrossRef](#)]
11. Rignot, E.; Thomas, R.H. Mass Balance of Polar Ice Sheets. *Science* **2002**, *297*, 1502–1506. [[CrossRef](#)]
12. Zwally, H.J.; Giovinetto, M.B.; Li, J.; Cornejo, H.G.; Beckley, M.A.; Brenner, A.C.; Saba, J.L.; Yi, D. Mass Changes of the Greenland and Antarctic Ice Sheets and Shelves and Contributions to Sea-Level Rise: 1992–2002. *J. Glaciol.* **2005**, *51*, 509–527. [[CrossRef](#)]
13. Tapley, B.D.; Bettadpur, S.; Ries, J.C.; Thompson, P.F.; Watkins, M.M. GRACE Measurements of Mass Variability in the Earth System. *Science* **2004**, *305*, 503–505. [[CrossRef](#)]
14. Rignot, E.; Bamber, J.L.; van den Broeke, M.R.; Davis, C.; Li, Y.; van de Berg, W.J.; van Meijgaard, E. Recent Antarctic Ice Mass Loss from Radar Interferometry and Regional Climate Modelling. *Nat. Geosci.* **2008**, *1*, 106–110. [[CrossRef](#)]
15. Rignot, E.; Velicogna, I.; van den Broeke, M.R.; Monaghan, A.; Lenaerts, J.T.M. Acceleration of the Contribution of the Greenland and Antarctic Ice Sheets to Sea Level Rise: Acceleration of Ice Sheet Loss. *Geophys. Res. Lett.* **2011**, *38*, L05503. [[CrossRef](#)]
16. Gardner, A.S.; Moholdt, G.; Scambos, T.; Fahnestock, M.; Ligtenberg, S.; van den Broeke, M.; Nilsson, J. Increased West Antarctic and Unchanged East Antarctic Ice Discharge over the Last 7 Years. *Cryosphere* **2018**, *12*, 521–547. [[CrossRef](#)]

17. Shen, Q.; Wang, H.; Shum, C.K.; Jiang, L.; Hsu, H.T.; Dong, J. Recent High-Resolution Antarctic Ice Velocity Maps Reveal Increased Mass Loss in Wilkes Land, East Antarctica. *Sci. Rep.* **2018**, *8*, 4477. [CrossRef]
18. Li, X.; Rignot, E.; Mouginot, J.; Scheuchl, B. Ice Flow Dynamics and Mass Loss of Totten Glacier, East Antarctica, from 1989 to 2015. *Geophys. Res. Lett.* **2016**, *43*, 6366–6373. [CrossRef]
19. Zhou, C.; Liang, Q.; Chen, Y.; Lei, H.; Fu, Z.; Zheng, L.; Liu, R. Mass Balance Assessment of the Amery Ice Shelf Basin, East Antarctica. *Earth Space Sci.* **2019**, *6*, 1987–1999. [CrossRef]
20. Cui, X.; Du, W.; Xie, H.; Sun, B. The Ice Flux to the Lambert Glacier and Amery Ice Shelf along the Chinese Inland Traverse and Implications for Mass Balance of the Drainage Basins, East Antarctica. *Polar Res.* **2020**, *39*, 3582. [CrossRef]
21. Xu, D.; Tang, X.; Yang, S.; Zhang, Y.; Wang, L.; Li, L.; Sun, B. Revisiting Ice Flux and Mass Balance of the Lambert Glacier–Amery Ice Shelf System Using Multi-Remote-Sensing Datasets, East Antarctica. *Remote Sens.* **2022**, *14*, 391. [CrossRef]
22. Selley, H.L.; Hogg, A.E.; Cornford, S.; Dutrieux, P.; Shepherd, A.; Wuite, J.; Floricioiu, D.; Kusk, A.; Nagler, T.; Gilbert, L.; et al. Widespread Increase in Dynamic Imbalance in the Getz Region of Antarctica from 1994 to 2018. *Nat. Commun.* **2021**, *12*, 1133. [CrossRef]
23. Diener, T.; Sasgen, I.; Agosta, C.; Fürst, J.J.; Braun, M.H.; Konrad, H.; Fettweis, X. Acceleration of Dynamic Ice Loss in Antarctica From Satellite Gravimetry. *Front. Earth Sci.* **2021**, *9*, 741789. [CrossRef]
24. Mouginot, J.; Rignot, E.; Scheuchl, B.; Millan, R. Comprehensive Annual Ice Sheet Velocity Mapping Using Landsat-8, Sentinel-1, and RADARSAT-2 Data. *Remote Sens.* **2017**, *9*, 364. [CrossRef]
25. Gardner, A.S.; Fahnestock, M.A.; Scambos, T.A. *MEaSURES ITS_LIVE Landsat Image-Pair Glacier and Ice Sheet Surface Velocities: Version 1*; National Snow and Ice Data Center: Boulder, CO, USA, 2019. [CrossRef]
26. Scheuchl, B.; Mouginot, J.; Rignot, E. *MEaSURES InSAR-Based Ice Velocity Maps of Central Antarctica: 1997 and 2009, Version 1*; NASA National Snow and Ice Data Center Distributed Active Archive Center: Boulder, CO, USA, 2012. [CrossRef]
27. Rignot, E.; Mouginot, J.; Scheuchl, B. *MEaSURES InSAR-Based Antarctica Ice Velocity Map, Version 2*. [Indicate Subset Used]; NASA National Snow and Ice Data Center Distributed Active Archive Center: Boulder, CO, USA, 2017. [CrossRef]
28. Rignot, E.; Mouginot, J.; Scheuchl, B.; Jeong, S. Changes in Antarctic Ice Sheet Motion Derived From Satellite Radar Interferometry Between 1995 and 2022. *Geophys. Res. Lett.* **2022**, *49*, e2022GL100141. [CrossRef]
29. Zwally, H.J.; Giovinetto, M.B.; Beckley, M.A.; Saba, J.L. Antarctic and Greenland Drainage Systems. GSFC Cryospheric Sciences Laboratory. 2012. Available online: http://icesat4.gsfc.nasa.gov/cryo_data/ant_grn_drainage_systems.php (accessed on 30 May 2022).
30. Depoorter, M.A.; Bamber, J.L.; Griggs, J.A.; Lenaerts, J.T.M.; Ligtenberg, S.R.M.; van den Broeke, M.R.; Moholdt, G. Calving Fluxes and Basal Melt Rates of Antarctic Ice Shelves. *Nature* **2013**, *502*, 89–92. [CrossRef]
31. Griggs, J.A.; Bamber, J.L. Antarctic Ice-Shelf Thickness from Satellite Radar Altimetry. *J. Glaciol.* **2011**, *57*, 485–498. [CrossRef]
32. Morlighem, M.; Rignot, E.; Seroussi, H.; Larour, E.; Ben Dhia, H.; Aubry, D. A Mass Conservation Approach for Mapping Glacier Ice Thickness: BALANCE THICKNESS. *Geophys. Res. Lett.* **2011**, *38*. [CrossRef]
33. Agosta, C.; Amory, C.; Kittel, C.; Orsi, A.; Favier, V.; Gallée, H.; van den Broeke, M.R.; Lenaerts, J.T.M.; van Wessem, J.M.; van de Berg, W.J.; et al. Estimation of the Antarctic Surface Mass Balance Using the Regional Climate Model MAR (1979–2015) and Identification of Dominant Processes. *Cryosphere* **2019**, *13*, 281–296. [CrossRef]
34. Gossart, A.; Helsen, S.; Lenaerts, J.T.M.; Broucke, S.V.; van Lipzig, N.P.M.; Souverijns, N. An Evaluation of Surface Climatology in State-of-the-Art Reanalyses over the Antarctic Ice Sheet. *J. Clim.* **2019**, *32*, 6899–6915. [CrossRef]
35. Wessem, J.M.V.; van de Berg, W.J.; Noël, B.P.Y.; van Meijgaard, E.; Amory, C.; Birnbaum, G.; Jakobs, C.L.; Krüger, K.; Lenaerts, J.T.M.; Lhermitte, S.; et al. Modelling the Climate and Surface Mass Balance of Polar Ice Sheets Using RACMO2—Part 2: Antarctica (1979–2016). *Cryosphere* **2018**, *12*, 1479–1498. [CrossRef]
36. Lenaerts, J.T.M.; Medley, B.; van den Broeke, M.R.; Wouters, B. Observing and Modeling Ice Sheet Surface Mass Balance. *Rev. Geophys.* **2019**, *57*, 376–420. [CrossRef]
37. Wessem, J.M.V.; Reijmer, C.H.; Morlighem, M.; Mouginot, J.; Rignot, E.; Medley, B.; Joughin, I.; Wouters, B.; Depoorter, M.A.; Bamber, J.L.; et al. Improved Representation of East Antarctic Surface Mass Balance in a Regional Atmospheric Climate Model. *J. Glaciol.* **2014**, *60*, 761–770. [CrossRef]
38. Mohajerani, Y.; Velicogna, I.; Rignot, E. Mass Loss of Totten and Moscow University Glaciers, East Antarctica, Using Regionally Optimized GRACE Mascons. *Geophys. Res. Lett.* **2018**, *45*, 7010–7018. [CrossRef]
39. Mohajerani, Y.; Velicogna, I.; Rignot, E. Evaluation of Regional Climate Models Using Regionally Optimized GRACE Mascons in the Amery and Getz Ice Shelves Basins, Antarctica. *Geophys. Res. Lett.* **2019**, *46*, 13883–13891. [CrossRef]
40. Muñoz-Sabater, J.; Dutra, E.; Agustí-Panareda, A.; Albergel, C.; Arduini, G.; Balsamo, G.; Boussetta, S.; Choulga, M.; Harrigan, S.; Hersbach, H.; et al. ERA5-Land: A State-of-the-Art Global Reanalysis Dataset for Land Applications. *Earth Syst. Sci. Data* **2021**, *13*, 4349–4383. [CrossRef]
41. Haran, T.; Klinger, M.; Bohlander, J.; Fahnestock, M.; Painter, T.; Scambos, T. *MEaSURES MODIS Mosaic of Antarctica 2013–2014 (MOA2014) Image Map, Version 1*. [Surface Morphology]; NASA National Snow and Ice Data Center Distributed Active Archive Center: Boulder, CO, USA, 2018. [CrossRef]
42. Cheng, Y.; Xia, M.; Qiao, G.; Lv, D.; Li, Y.; Hai, G. Imminent Calving Accelerated by Increased Instability of the Brunt Ice Shelf, in Response to Climate Warming. *Earth Planet. Sci. Lett.* **2021**, *572*, 117132. [CrossRef]

43. Mottram, R.; Hansen, N.; Kittel, C.; van Wessem, J.M.; Agosta, C.; Amory, C.; Boberg, F.; van de Berg, W.J.; Fettweis, X.; Gossart, A.; et al. What Is the Surface Mass Balance of Antarctica? An Intercomparison of Regional Climate Model Estimates. *Cryosphere* **2021**, *15*, 3751–3784. [[CrossRef](#)]
44. Conway, H.; Rasmussen, L.A. Recent Thinning and Migration of the Western Divide, Central West Antarctica. *Geophys. Res. Lett.* **2009**, *36*, L12502. [[CrossRef](#)]
45. Deb, P.; Orr, A.; Bromwich, D.H.; Nicolas, J.P.; Turner, J.; Hosking, J.S. Summer Drivers of Atmospheric Variability Affecting Ice Shelf Thinning in the Amundsen Sea Embayment, West Antarctica. *Geophys. Res. Lett.* **2018**, *45*, 4124–4133. [[CrossRef](#)]
46. Kang, J.; Lu, Y.; Li, Y.; Zhang, Z.; Shi, H. Antarctic Basal Water Storage Variation Inferred from Multi-Source Satellite Observation and Relevant Models. *Remote Sens.* **2022**, *14*, 2337. [[CrossRef](#)]
47. Artemieva, I.M. Antarctica Ice Sheet Basal Melting Enhanced by High Mantle Heat. *Earth-Sci. Rev.* **2022**, *226*, 103954. [[CrossRef](#)]
48. Miles, B.W.J.; Stokes, C.R.; Jamieson, S.S.R.; Jordan, J.R.; Gudmundsson, G.H.; Jenkins, A. High Spatial and Temporal Variability in Antarctic Ice Discharge Linked to Ice Shelf Buttressing and Bed Geometry. *Sci. Rep.* **2022**, *12*, 10968. [[CrossRef](#)] [[PubMed](#)]
49. Cheng, Y.; Xia, M.; Qiao, G.; Li, Y.; Hai, G.; Lv, D. Calving Cycle of Ninnis Glacier over the Last 60 Years. *Int. J. Appl. Earth Obs. Geoinf.* **2021**, *105*, 102612. [[CrossRef](#)]
50. Thoma, M.; Jenkins, A.; Holland, D.; Jacobs, S. Modelling Circumpolar Deep Water Intrusions on the Amundsen Sea Continental Shelf, Antarctica. *Geophys. Res. Lett.* **2008**, *35*, L18602. [[CrossRef](#)]
51. Jacobs, S.S.; Jenkins, A.; Giulivi, C.F.; Dutrieux, P. Stronger Ocean Circulation and Increased Melting under Pine Island Glacier Ice Shelf. *Nat. Geosci.* **2011**, *4*, 519–523. [[CrossRef](#)]
52. MacGregor, J.A.; Catania, G.A.; Markowski, M.S.; Andrews, A.G. Widespread Rifting and Retreat of Ice-Shelf Margins in the Eastern Amundsen Sea Embayment between 1972 and 2011. *J. Glaciol.* **2012**, *58*, 458–466. [[CrossRef](#)]
53. Scott, R.C.; Nicolas, J.P.; Bromwich, D.H.; Norris, J.R.; Lubin, D. Meteorological Drivers and Large-Scale Climate Forcing of West Antarctic Surface Melt. *J. Clim.* **2019**, *32*, 665–684. [[CrossRef](#)]
54. Bodart, J.A.; Bingham, R.J. The Impact of the Extreme 2015–2016 El Niño on the Mass Balance of the Antarctic Ice Sheet. *Geophys. Res. Lett.* **2019**, *46*, 13862–13871. [[CrossRef](#)]

Disclaimer/Publisher’s Note: The statements, opinions and data contained in all publications are solely those of the individual author(s) and contributor(s) and not of MDPI and/or the editor(s). MDPI and/or the editor(s) disclaim responsibility for any injury to people or property resulting from any ideas, methods, instructions or products referred to in the content.